COMMUNICATIONS

Conformation of the Glycosidic Linkage in a Disaccharide Investigated by Double-Quantum Solid-State NMR

S. Ravindranathan,*,[1] T. Karlsson,*,[2] K. Lycknert,† G. Widmalm,† and M. H. Levitt*

*Physical Chemistry Division, and †Department of Organic Chemistry, Stockholm University, S-10691 Stockholm, Sweden

E-mail: mhl@physc.su.se

Double-quantum heteronuclear local field NMR is performed on a sample of a $^{13}C_2$-labeled disaccharide, in which the two ^{13}C spins are located on opposite sides of the glycosidic linkage. The evolution of the double-quantum coherences is found to be consistent with the solid-state conformation of the molecule, as previously determined by X-ray diffraction. The dependence of the double-quantum evolution on the glycosidic torsional angles is examined by using a graphical molecular manipulation program interfaced to a numerical spin simulation module. © 2001 Academic Press

Key Words: **double-quantum NMR; carbohydrates; glycosidic linkage; trehalose; Moleculix.**

1. INTRODUCTION

Carbohydrates are an important class of molecules that play a wide range of functional and structural roles in biological systems (*1*). In order to understand their behavior, one requires detailed knowledge of their molecular structure. In oligosaccharides and polysaccharides, the conformation of the glycosidic linkage joining neighboring sugar rings is of particular importance. The conformation of the glycosidic linkage defines the relative orientation of neighboring rings and hence the three-dimensional structure of the molecule.

There are a number of NMR methods for investigating the conformation of the glycosidic linkage. In solution, it is possible to estimate distances between pairs of protons on opposite sides of the linkage through their mutual cross-relaxation (*2, 3*). However, it is difficult to obtain enough distance constraints to define the glycosidic conformation accurately. A different method involves the measurement of three-bond indirect coupling constants, such as $^3J_{CH}$ and $^3J_{CC}$, followed by appli-

cation of the appropriate Karplus relationship (*4–7*). Carbohydrate conformation may also be investigated by measuring residual through-space spin–spin couplings in weakly oriented solutions (*8–10*) or by exploiting cross-correlated relaxation effects (*11–13*). Cross-correlation effects have also been exploited to assist the assignment of carbohydrate solution spectra (*14*). However, all solution NMR methods are limited to molecules with rapid rotational motion and are difficult to apply to many polymeric systems or large glycoconjugates.

In principle, solid-state NMR, in conjunction with selective isotopic enrichment of the sites of interest, may be used to estimate molecular conformations without restrictions on the rotational mobility. For example, the conformation of the disaccharide α, α'-trehalose has been investigated in the glassy state by magic-angle-spinning ^{13}C NMR. The isotropic ^{13}C chemical shifts could be related to the glycosidic conformational angles with the help of *ab initio* quantum calculations (*15*).

It is also possible to estimate molecular geometries by measuring the relative orientations of spin interaction tensors in the solid state (*12, 16–27*). A particularly promising tool for investigating carbohydrate conformations is HCCH-2Q-HLF (heteronuclear local field) spectroscopy (*12, 16–19*). This experiment estimates the angles between pairs of ^{13}C–^1H vectors by allowing $^{13}C_2$ double-quantum coherences to evolve under the local fields generated by neighboring protons. The experiment has been employed successfully in large molecular systems, such as membrane proteins (*17, 18*). Since carbohydrates are rich in methine groups, the HCCH-2Q-HLF experiment has wide potential applications in carbohydrate chemistry. As reported in a recent paper (*12*), HCCH-2Q-HLF experiments on [1,2-$^{13}C_2$]-labeled glucose are clearly capable of distinguishing between the α and β anomers. A successful experiment has also been performed on a [1,3-$^{13}C_2$]-labeled monosaccharide, in which the two ^{13}C nuclei are separated by a distance of 0.249 nm (*12*).

This Communication reports the first application of HCCH-2Q-HLF spectroscopy to pairs of ^{13}C sites spanning the
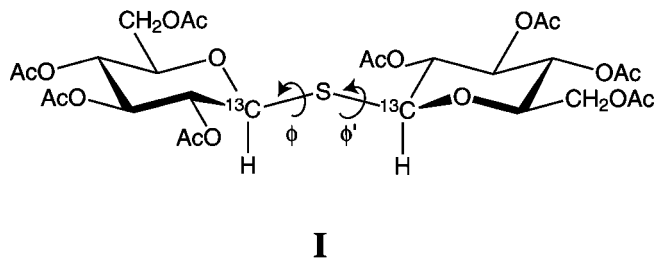
FIG. 1. The molecular structure of octa-O-acetyl-β,β'-thio-[1,1'-$^{13}C_2$]-trehalose. The glycosidic conformation is defined by the torsional angles $\phi = \phi_{OCSC'}$ and $\phi' = \phi_{CSC'O'}$.

glycosidic linkage in a disaccharide. The system chosen is octa-O-acetyl-β,β'-thio-[1,1'-$^{13}C_2$]-trehalose, henceforth referred to as **I** (see Fig. 1). The glycosidic conformation is defined by the two torsional angles $\phi_{OCSC'}$ (henceforth referred to as ϕ), and $\phi_{CSC'O'}$ (henceforth referred to as ϕ'). The substance **I** was chosen because the synthesis is relatively straightforward and because the crystal structure has been determined by X-ray diffraction (28). The X-ray structure corresponds to the conformation $(\phi, \phi') = (-67.2°, -117.1°)$, with the two ^{13}C sites separated by 0.269 nm. The value of ϕ' is fairly unusual since the CS and C'H bonds are almost eclipsed. The eclipsed solid-state conformation may be contrasted with the staggered conformation $(\phi, \phi') \cong (-61°, -61°)$, which molecular dynamics simulations have predicted to be heavily populated in solution (29).

The purpose of this study is (i) to verify that HCCH-2Q-HLF may indeed be applied to $^{13}C_2$ pairs straddling the glycosidic linkage, and (ii) to assess how much information on the glycosidic conformation is obtained by a single HCCH-2Q-HLF experiment. In particular, it is interesting to see whether the HCCH-2Q-HLF experiment is capable of detecting the unusual value of ϕ' in the crystalline state.

2. SAMPLE PREPARATION

2,3,4,6-Tetra-O-acetyl-α-[1-^{13}C]-glucopyranosyl bromide was prepared from D-α-[1-^{13}C]-glucose (Omicron Biochemicals, Inc., IN, USA) using the procedure described by Lemieux (30). The 2,3,4,6-tetra-O-acetyl-α-D-[1-^{13}C]-glucopyranosyl bromide was combined with H_2S to yield octa-O-acetyl β,β'-thio-[1,1'-$^{13}C_2$]-trehalose (**I**) as described in Ref. (31). The $^{13}C_2$-labeled disaccharide was crystallized from ethanol at ambient temperature. The ^1H NMR spectrum of a solution of β,β'-thio-[1,1'-$^{13}C_2$]-trehalose in $CDCl_3$ at 30°C, recorded on a JEOL 270 MHz spectrometer, showed spin–spin couplings of $^3J_{H1,H2} = 10.2$ Hz, $^1J_{H1,C1} = 160$ Hz, and a transglycosidic $^3J_{CH}$ coupling constant of 3.7 Hz.

The nonlabeled disaccharide was prepared from nonlabeled materials in the same way. An isotopically diluted sample of **I** was prepared by cocrystallizing the $^{13}C_2$-labeled and nonlabeled substances from ethanol. The diluted sample contained 20% of the $^{13}C_2$-labeled compound. The total mass of the NMR sample was around 80 mg.

3. SOLID-STATE NMR

All solid-state NMR experiments were performed at ambient temperature in a static magnetic field of 9.4 T using standard 4-mm triple-resonance magic-angle spinning probe and a CMX-400 infinity spectrometer (Varian Instruments). A spinning frequency of 5523 Hz was used throughout. The cross-polarization interval was 5.0 ms. The RF fields during cross polarization corresponded to a nutation frequency of 50 kHz. An interval of 90s was allowed for recovery of the ^1H magnetization between successive transients. The proton decoupler field during ^{13}C signal acquistion corresponded to a nutation frequency of 68 kHz.

3.1. One-Dimensional Spectra

Figure 2a shows a solid-state ^{13}C spectrum of the isotopically diluted sample of **I**. The spectrum shows two strong peaks from the labeled ^{13}C sites as well as weaker signals from the natural abundance spins. The small isotropic shift difference of 0.9 ppm between the two strong ^{13}C peaks is due to the asymmetry of the molecules in the crystal structure (28).

Figure 2b shows a double-quantum-filtered spectrum of the same compound under identical conditions, obtained using the C7 pulse sequence (32). The duration of the double-quantum excitation and reconversion intervals were both $\tau_{exc} = 3357$ μs. The ^{13}C and ^1H RF fields during the double-quantum excitation
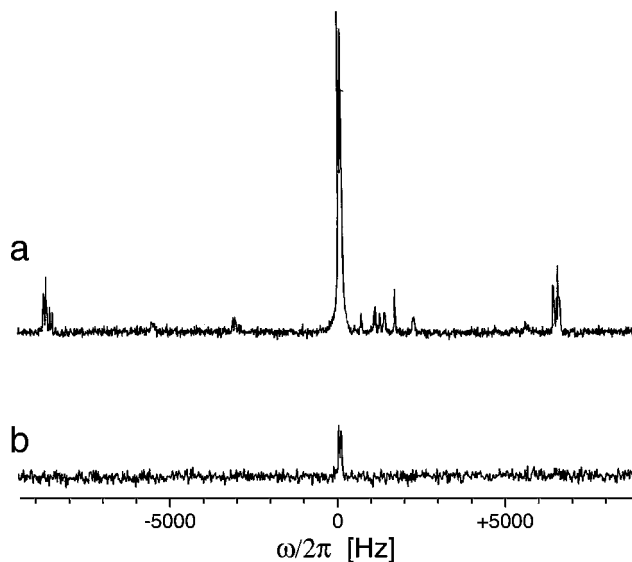

FIG. 2. (a) ^{13}C spectrum of a crystalline sample of **I**, diluted to a level of 20% in unlabeled material, obtained at a magnetic field of $B_0 = 9.4$ T using cross polarization at a spinning frequency of $\omega_r/2\pi = 5523$ Hz. The weaker peaks are from natural ^{13}C spins. (b) Double-quantum-filtered ^{13}C spectrum of the isotopically diluted sample of **I**, using conditions identical to those of (a), but using a C7 pulse sequence of duration $\tau_{exc} = 3357$ μs to excite 2Q coherences and a second C7 pulse sequence of identical duration to recover observable magnetization. Phase cycling was used to suppress signals not passing through double-quantum coherence. The spectrum only shows signals from the introduced $^{13}C_2$ pairs.

corresponded to nutation frequencies of 38 and 89 kHz, respectively.

Figure 2b shows two signals from the labeled sites, with complete suppression of the signals from isolated ^{13}C spins. The double-quantum filtering efficiency (32) is estimated to be around 8%. This figure is rather disappointing, even for the rather long ^{13}C...^{13}C distance of ~0.269 nm. In the present case, it was difficult to optimize the double-quantum excitation because of the long ^{1}H spin–lattice relaxation time constant of at least 20 s. Recent experience with new double-quantum excitation sequences (33) suggests that far larger double-quantum efficiencies should be achievable at this ^{13}C–^{13}C distance.

3.2. Double-Quantum Heteronuclear Local Field Spectroscopy

The HCCH-2Q-HLF experiment has already been described elsewhere (12, 16–19). The current experiments employed the pulse sequence given in Ref. (12). Briefly, the experiment uses a standard ramped cross-polarization sequence (34), followed by a $\pi/2$ pulse, to enhance the longitudinal ^{13}C magnetization, which is converted into ^{13}C$_2$ double-quantum coherences using a C7 pulse sequence (32) of duration τ_{exc}. The double-quantum ^{13}C$_2$ coherences are allowed to evolve for an interval t_1 under the heteronuclear local fields from the neighboring protons. Homonuclear proton–proton couplings are suppressed during the interval t_1 by applying a suitable pulse sequence on the proton channel. The ^{13}C$_2$ double-quantum coherences are reconverted into observable single-quantum coherences by applying a second C7 sequence of duration τ_{exc}, followed by a $\pi/2$ pulse. The experiment is repeated for a small number of evolution intervals t_1.

Figure 3 shows a set of experimental results for the isotopically diluted sample of **I**, using double-quantum excitation and
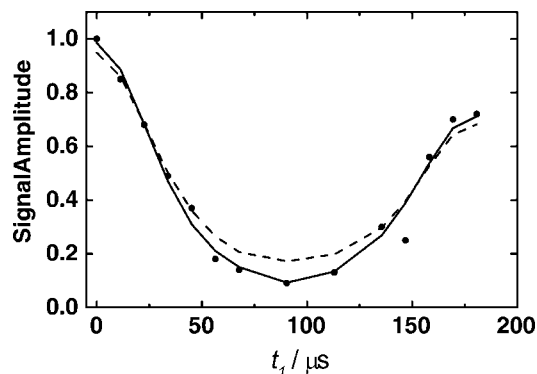

FIG. 3. (solid circles) Experimental integrated peak amplitudes for the HCCH-2Q-HLF experiment on the isotopically diluted sample of **I**, normalized so that the point for $t_1 = 0$ has unit amplitude. The measured error margins of the spectral integrals are less than the size of the solid circles. In practice, instrumental instabilities and systematic errors dominate. (solid line) Best-fit four-spin simulation for the X-ray geometry $(\phi, \phi') = (-67.2°, -117.1°)$. (dashed line) Best-fit four-spin simulation for the putative solution-state geometry $(\phi, \phi') = (-61.0°, -61.0°)$.

reconversion intervals of $\tau_{\text{exc}} = 3357$ μs. The ^{13}C and ^{1}H RF fields during the double-quantum excitation corresponded to nutation frequencies of 38 and 89 kHz, respectively. The MREV8 sequence was used (35) for proton–proton decoupling, with a nutation frequency of 83 kHz. Each experimental point represents the integrated double-quantum-filtered spectral amplitude for a particular value of the evolution interval t_1. Thirty-two transients were collected for each increment of t_1. At first, the experimental amplitudes decrease as t_1 is incremented, but then recover to form a rotational echo when t_1 approaches a full rotational period $\tau_r = |2\pi/\omega_r|$.

Analysis of the HCCH-2Q-HLF results requires an estimate of the scaling factor κ for the MREV8 sequence, as described in Ref. (12). The scaling factor was calibrated by performing the HCCH-2Q-HLF on a sample of β-[1,2-^{13}C$_2$]-glucose, under conditions identical to that used for the sample of **I**, except for the double-quantum excitation and reconversion intervals, which had a duration of $\tau_{\text{exc}} = 620$ μs. Simulations using the known geometrical parameters for β-[1,2-^{13}C$_2$]-glucose, as described in Ref. (12), gave a calibrated multiple-pulse scaling factor of $\kappa = 0.45$.

4. SIMULATIONS

We performed simulations of the HCCH-2Q-HLF experiment using the dipole–dipole interactions within the four-spin-$\frac{1}{2}$ system formed by the two ^{13}C labels and the two attached protons. The chemical shift anisotropies were not included since the HCCH-2Q-HLF experiment is highly insensitive to these interactions (12, 16–19). The homonuclear interaction between the two ^{13}C spins is involved in the excitation of the double-quantum coherences, but does not participate in the evolution of those coherences during t_1.

A graphical package, called `Moleculix`, was written using an interactive graphical interface (36, 37). This package depicts the three-dimensional molecular structure, and allows torsional angles or bond angles to be changed interactively. Chemical shift tensors or other spin interactions may be attached to local molecular fragments. As the molecular structure changes, the magnitudes and orientations of dipole–dipole coupling interactions, and the orientations of chemical shift tensors, are recalculated dynamically. The `Moleculix` package interfaces to a selection of NMR simulation routines.

In the present case, `Moleculix` was used to construct a graphical model of the molecule **I** using the X-ray coordinates (28). The torsional angles ϕ and ϕ' were then varied, keeping bond lengths and bond angles fixed. The recalculated dipole–dipole couplings were used to perform new HCCH-2Q-HLF simulations. The simulated curves were fitted to the experimental results by scaling them vertically using a numerical factor A, and by multiplication with an exponential decay function, using a decay rate constant λ (12).

The geometry of the four-spin unit was defined using the bond angles $\theta_{\text{H–C–S}} = 109.93°$, $\theta_{\text{S–C'–H'}} = 109.61°$, and the

bond lengths C–H = 0.113 nm, C–S = 0.1781 nm, and S–C' = 0.1784 nm. The distance between the ^{13}C spins was 0.269 nm, independent of the torsional angles ϕ and ϕ'. The value of 0.113 nm for the effective C–H bond length is consistent with the librational averaging of the ^{1}H–^{13}C dipolar interactions (38). As discussed in Ref. (12), the precise values of the one-bond ^{1}H–^{13}C dipolar interactions are unimportant for the torsional angle estimation.

The fit of the simulations to the experimental data was assessed by computing the χ^2 statistic, defined by

$$\chi^2 = \sum_{i=1}^{N} \left(a_i^{\text{sim}} - a_i^{\text{exp}}\right)/\sigma^2, \qquad [1]$$

where a_i^{sim} and a_i^{exp} are the simulated and experimental points respectively, and the sum is over all N experimental points. Since the experimental errors are dominated in this case by instrumental instabilities rather than thermal noise, the variance σ^2 was defined according to the recommended procedure in Press et al. (39),

$$\sigma^2 = \sum_{i=1}^{N} \left(a_i^{\text{best sim}} - a_i^{\text{exp}}\right)/(N - M), \qquad [2]$$

where $a_i^{\text{best sim}}$ represents the simulated points at the global best fit, and M is the number of fit parameters. In the present case, $N = 14$ and $M = 2$. With this definition, the confidence limit on a fit parameter may be estimated by taking the parameter range for which χ^2 is less than $(N - M)\sqrt{2} = 12\sqrt{2}$ (39).

The solid line in Fig. 3 shows the best fit simulation for the X-ray geometry $(\phi, \phi') = (-67.2°, -117.1°)$. The match with the experimental data is good, except for a single data point, which was possibly disturbed by instrumental instabilities.

Molecular dynamics simulations (29) predict that the major conformation in solution is expected to be symmetrical, with torsional angles close to $(\phi, \phi') = (-61.0°, -61.0°)$. The best-fit simulation for this geometry is shown by the dashed line in Fig. 3. The fit is significantly poorer than for the true crystal geometry.

A contour plot of χ^2 against the torsional angles ϕ and ϕ' is shown in Fig. 4. This plot shows that the X-ray conformation $(\phi, \phi') = (-67.2°, -117.1°)$ lies close to a region of minimal χ^2 and that many feasible geometries, including the region around $(\phi, \phi') = (-60°, -60°)$, are clearly excluded. However, this plot also shows that there are many possible geometries that fit the experimental data equally well.

This point is emphasized by Fig. 5, which shows the variation of χ^2 against either ϕ or ϕ', with the other torsional angle kept fixed. These curves display multiple minima and several broad regions in which the simulated data are insensitive to the geometrical parameter. The dashed line shows the threshold $\chi^2 = 12\sqrt{2}$ below which the deviations between experimental and simulated curves are statistically insignificant.
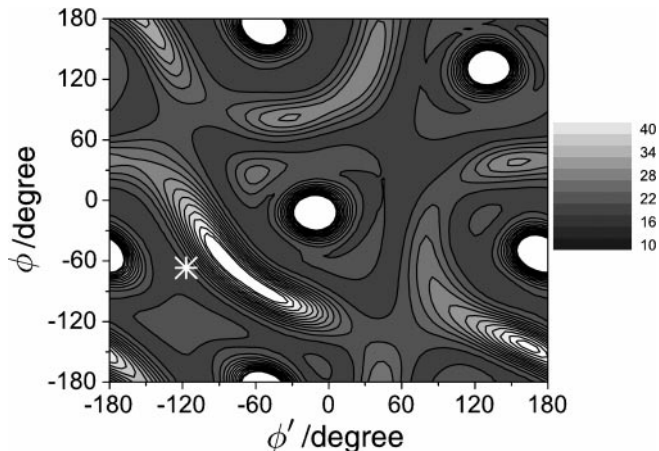

FIG. 4. Contour plot of χ^2 against the two torsional angles ϕ and ϕ'. Dark regions represent low values of χ^2. The X-ray conformation $(\phi, \phi') = (-67.2°, -117.1°)$ is indicated by a star.

These plots show that the HCCH-2Q-HLF experiment is capable of ruling out certain geometries but is not capable of tying down the glycosidic conformation by itself. This is not surprising since the spin dynamics are mainly sensitive to the angle subtended by the two direct ^{13}C–^{1}H vectors, and there are many combinations of ϕ and ϕ' that provide the same intervector angle.
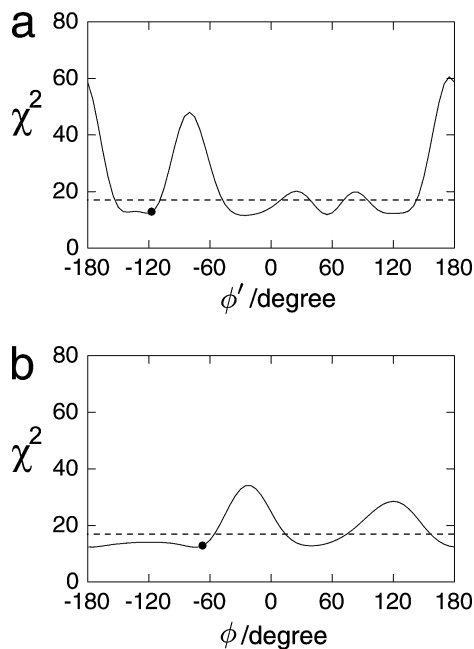

FIG. 5. (a) Plot of χ^2 (arbitrary units) against the torsional angle ϕ, with ϕ' fixed at $-117.1°$. (b) Plot of χ^2 (arbitrary units) against the torsional angle ϕ', with ϕ fixed at $-67.2°$. In both plots, the X-ray conformation is indicated by a solid circle. The line $\chi^2 = 12\sqrt{2}$ is indicated by a dashed line. Below this line, deviations between experimental results and simulations are not significant.

5. CONCLUSIONS

We have performed for the first time a HCCH-2Q-HLF angular determination experiment across the glycosidic linkage in a disaccharide. The experiment is able to rule out certain molecular conformations, but a single experiment of this type provides highly ambiguous angular information and is not expected to be very useful on its own.

Much more detailed information on the molecular geometry may be obtained by (i) combining the HCCH-2Q-HLF experiments with analyses of the chemical shifts, of the type described in Ref. (*15*), or (ii) combinations of many different HCCH-2Q-HLF measurements, using a selection of $^{13}C_2$ pairs at different positions. For example, if there is sufficient signal strength, it should be possible to use a sample labeled at only one ^{13}C position. Double-quantum coherences could be excited between the labeled site and natural ^{13}C spins in the rest of the molecule. This would provide a wealth of complementary angular information.

Experiments of this type are likely to be useful for obtaining molecular geometrical information on complex system such as polysaccharides and glycoproteins. Although the sensitivity achieved in this first experiment is relatively poor, advances in dipolar recoupling methodology are likely to improve matters in the future (*32, 33, 40–42*). The conformational distributions that are likely to be encountered in complex systems will create complications, but these might be resolved in an informative way by combining several types of complementary NMR data. For example, the full two-dimensional HCCH-2Q-HLF spectrum contains plentiful information on the conformational distribution, through the correlation of the isotropic chemical shifts and the 2Q evolution curves.

REFERENCES

1. H. J. Gabius and S. Gabius, "Glycosciences," Chapman and Hall, London (1997).

2. G. Widmalm, A. Byrd, and W. Egan, A conformational study of $\alpha - L - $ Rha$p - (1 \rightarrow 2) - \alpha - L - $ Rha$p - (1 \rightarrow $ OMe) by NMR nuclear Overhauser spectroscopy (NOESY) and molecular dynamics calculations, *Carbohydr. Res.* **229,** 195–211 (1992).

3. J. H. Prestegard, T. A. W. Koerner, Jr., P. C. Demou, and R. K. Yu, Complete analysis of oligosaccharide primary structure using 2-D high field ^{1}H NMR, *J. Am. Chem. Soc.* **104,** 4993–4995 (1982).

4. T. Rundlöf, A. Kjellberg, C. Damberg, T. Nishida, and G. Widmalm, Long range proton–carbon coupling constants in conformational analysis of oligosaccharides, *Magn. Reson. Chem.* **35,** 839–847 (1998).

5. B. Bose, S. Zhao, R. Stenutz, F. Cloran, P. B. Bondo, B. Hertz, I. Carmichael, and S. Seriani, Three bond C–O–C–C spin-coupling constants in carbohy-

6. D. Uhrin, A. Mele, K. E. Kövér, J. Boyd, and R. A. Dwek, One-dimensional inverse-detected methods for measurement of long-range proton-carbon coupling constants. Applications to saccharides, *J. Magn. Reson. A* **108,** 160–170 (1994).

7. I. Tvaroska and F. R. Taravel, Carbon-proton coupling constants in the conformational analysis of sugar molecules, *Adv. Carbohydr. Chem. Biochem.* **51,** 15–61 (1995).

8. T. Rundlöf, C. Landersjö, K. Lycknert, A. Maliniak, and G. Widmalm, NMR investigation of oligosaccharide conformation using dipolar couplings in an aqueous dilute liquid crystalline medium, *Magn. Reson. Chem.* **35,** 773–776 (1998).

9. G. R. Kiddle and S. W. Homans, Residual dipolar couplings as new conformational restraints in isotopically ^{13}C-enriched oligosaccharides, *FEBS Lett.* **436,** 128–130 (1998).

10. P. J. Bolon and J. H. Prestegard, COSY cross-peaks from ^{1}H-^{1}H dipolar couplings in NMR spectra of field oriented oligosaccharides, *J. Am. Chem. Soc.* **120,** 9366–9367 (1998).

11. B. Reif, M. Hennig, and C. Griesinger, Direct measurement of angles between bond vectors in high resolution NMR, *Science* **276,** 1230–1233 (1997).

12. S. Ravindranathan, X. Feng, T. Karlsson, G. Widmalm, and M. H. Levitt, Investigation of carbohydrate conformation in solution and in powders by double quantum NMR, *J. Am. Chem. Soc.* **122,** 1102–1115 (2000).

13. P. Pelupessy, E. Chiarparin, and G. Bodenhausen, Simultaneous determination of Psi and Phi angles in proteins from measurements of cross-correlated relaxation effects, *J. Biomol. NMR* **14,** 277–280 (1999).

14. S. J. F. Vincent and C. Zwahlen, Dipole–dipole cross-correlation at ^{13}C natural abundance. A structural tool for polysaccharides, *J. Am. Chem. Soc.* **122,** 8307–8308 (2000).

15. P. Zhang, A. N. Klymachyov, S. Brown, J. G. Ellington, and P. J. Grandinetti, Solid-state ^{13}C NMR investigation of the glycosidic linkage in α-α' trehalose, *Solid State Nucl. Magn. Reson.* **12,** 221–225 (1998).

16. X. Feng, Y. K. Lee, D. Sandström, M. Edén, H. Maisel, A. Sebald, and M. H. Levitt, Direct determination of a molecular torsional angle by solid state NMR, *Chem. Phys. Lett.* **257,** 314–320 (1996).

17. X. Feng, P. J. E. Verdegem, Y. K. Lee, D. Sandström, M. Edén, P. Bovee-Geurts, W. J. de Grip, J. Lugtenburg, H. J. M. de Groot, and M. H. Levitt, Direct determination of a molecular torsional angle in the membrane protein rhodopsin by solid state NMR, *J. Am. Chem. Soc.* **119,** 6853–6857 (1997).

18. X. Feng, P. J. E. Verdegem, M. Edén, D. Sandström, Y. K. Lee, P. Bovee-Geurts, W. J. de Grip, J. Lugtenburg, H. J. M. de Groot, and M. H. Levitt, Determination of a molecular torsional angle in the metarhodopsin-I photointermediate of rhodopsin by double-quantum solid state NMR, *J. Biomol. NMR* **16,** 1–8 (2000).

19. D. A. Middleton, C. S. Le Duff, X. Peng, D. G. Reid, and D. Saunders, Molecular conformations of the polymorphic forms of cimetidine from ^{13}C solid-state NMR distance and angle measurements, *J. Am. Chem. Soc.* **122,** 1161–1170 (2000).

20. K. Schmidt-Rohr, A double quantum solid state NMR technique for determining torsion angles in polymers, *Macromolecules* **29,** 3975–3981 (1996).

21. K. Schmidt-Rohr, Torsion angle determination in solid ^{13}C-labelled amino acids and peptides by separated-local-field double-quantum NMR, *J. Am. Chem. Soc.* **118,** 7601–7603 (1996).

22. D. P. Weliky and R. Tycko, Determination of peptide conformations by 2-D MAS NMR exchange spectroscopy with rotor synchronization, *J. Am. Chem. Soc.* **118,** 8487–8488 (1996).

23. D. M. Gregory, M. A. Mehta, J. C. Shiels, and G. P. Drobny, Determination of local structure in solid nucleic acids using double quantum nuclear nuclear magnetic resonance spectroscopy, *J. Chem. Phys.* **107,** 28–42 (1997).

24. M. Hong, J. D. Gross, and R. G. Griffin, Site-resolved determination of peptide torsion angle ϕ from relative orientations of backbone N–H and C–H bonds by solid state NMR, *J. Phys. Chem. B* **101,** 5869–5874 (1997).

25. M. Hong, Determination of multiple ϕ-torsion angles in proteins by selective and extensive ^{13}C labelling and two-dimensional solid-state NMR, *J. Magn. Reson.* **139,** 389–401 (1999).

26. K. Takegoshi, T. Imaizumi, and T. Terao, One and two dimensional ^{13}C-^{1}H/^{15}N-^{1}H dipolar correlation experiments under fast magic angle spinning for determining the peptide dihedral angle ϕ, *Solid State Nucl. Magn. Reson.* **16,** 271–278 (2000).

27. J. D. van Beek, L. Beaulieu, H. Schäfer, M. Demura, T. Asakura, and B. H. Meier, Solid-state NMR determination of the secondary structure of *sami-acynthia ricini* silk, *Nature* **405,** 1077–1079 (2000).

28. M. Färnbäck, L. Eriksson, and G. Widmalm, Octa-O-acetylβ,β-thiotrehalose, *Acta Crystallogr. Sect. C* **56,** 700–701 (2000).

29. B. Stevensson, C. Höög, K. Ulfstedt-Jäkel, Z. Huang, G. Widmalm, and A. Maliniak, Solid-state deuterium NMR and molecular modelling studies of conformational dynamics in carbohydrates, *J. Phys. Chem. B* **104,** 6065–6070 (2000).

30. R. U. Lemieux, Tetra-*O*-Acetyl-α-D-glucopyranosyl bromide, *Meth. Carbohydr. Chem.* **2,** 221 (1963).

31. W. Schneider and F. Wrede, Synthese eines schwefelhaltigen und eines selenhaltigen disaccharides, *Ber. Deutsch. Chem. Ges.* **50,** 793–804 (1917).

32. Y. K. Lee, N. D. Kurur, M. Helmle, O. G. Johannessen, N. C. Nielsen, and M. H. Levitt, Efficient dipolar recoupling in the NMR of rotating solids. A seven fold symmetry radiofrequency pulse sequence, *Chem. Phys. Lett.* **242,** 304–309 (1995).

33. M. Carravetta, M. Eden, X. Zhao, A. Brinkmann, and M. H. Levitt, Symmetry principles for the design of radiofrequecy pulse sequences in the nuclear magnetic resonance of rotating solids, *Chem. Phys. Lett.* **321,** 205–215 (2000).

34. G. Metz, X. Wu, and S. O. Smith, Ramped-amplitude cross polarization in magic angle spinning NMR, *J. Magn. Reson. A* **110,** 219–227 (1994).

35. W. K. Rhim, D. D. Elleman, and R. W. Vaughan, Analysis of multipulse NMR in solids, *J. Chem. Phys.* **59,** 3740–3749 (1973).

36. T. Karlsson, N. Oyler, M. H. Levitt, and G. P. Drobny, Moleculix, an interactive visualization and simulation software package, Poster 135, 41st Experimental NMR Conference, Asilomar, California, April 2000.

37. The `Moleculix` package is written for Windows-NT and is available at the sites http://faculty.washington.edu/mtk and http://www.fos.su.se/~mhl.

38. Y. Ishii, T. Terao, and S. Hayashi, Theory and simulation of vibrational effects on structural measurements by solid-state nuclear magnetic resonance, *J. Chem. Phys.* **107,** 2760–2774 (1997).

39. W. H. Press, B. P. Flannery, S. A. Teukolsky, and W. T. Vetterling, "Numerical Recipes. The Art of Scientific Computing," Cambridge Univ. Press, Cambridge (1986).

40. A. Brinkmann, M. Edén, and M. H. Levitt, Synchronous Helical Pulse Sequences in Magic-Angle Spinning NMR. Double quantum recoupling of multiple-spin systems, *J. Chem. Phys.* **112,** 8539–8554 (2000).

41. T. Karlsson, M. Edén, H. Luthman, and M. H. Levitt, Efficient double-quantum excitation in rotational resonance NMR, *J. Magn. Reson.* **145,** 95–107 (2000).

42. T. Karlsson, C. E. Hughes, J. Schmedt auf der Günne, and M. H. Levitt, Double-quantum excitation in the NMR of spinning solids by pulse-assisted rotational resonance, *J. Magn. Reson.* **148,** 238–247 (2001).